A deeper insight into the influence of the electric field densities in Melt-Electrowriting: Printing in the 4th Dimension

*Rory Nairn, Orla Keenan, Uttariyo Saha, and Michael G. Monaghan**

R. N., U. S., O.K., Dr M.G. M.
Trinity Centre for Biomedical Engineering, Trinity Biomedical Sciences Institute, Trinity College Dublin, 152 - 160 Pearse Street, Dublin 2, Ireland
*E-mail: monaghmi@tcd.ie

Keywords: melt electrospinning writing, electric field modelling, additive manufacturing, material electrostatic interactions

Defined ordered structures for biomaterials and tissue engineering applications can be achieved by a variety of techniques, one of which includes the electrohydrodynamic (EHD)-based application of melt electrowriting (MEW), the extrusion of a molten polymer filament under pressure across a defined electric field. In this study, we investigate how to translate small fibre-meshes which are usually formed on flat surfaces, to curved contours that would have more applicability to human anatomical structures. By modelling the electric field strength associated with the MEW process, we found that incorporation of a non-conductive three-dimensional (3D) custom printed mould on the conductive collector plate offers the ability to accurately print patterns on non-flat surfaces successfully. Importantly, while the electric field strength is a constant in the MEW process; the electrostatic behaviour of the deposited polymer has the greatest impact on the accuracy of fibre patterning and stacking. Consequently, controlled fibre deposition was exhibited, provided that a constant electrical field strength and a continuous vertical distance between the nozzle and the mould is maintained.

Overall, this study establishes the groundwork to support further developments in MEW technologies, from flat to anatomically relevant 3D structures in the fields of regenerative medicine and biofabrication.

1. Introduction

Melt electrospinning writing (or melt electrowriting, MEW), is an advanced manufacturing process that produces finely-tuned scaffolds, and has shown promising application in tissue engineering and biomaterials science [1]. A standard MEW system constitutes a molten polymer extruded through a nozzle and collected at a grounded stage, moving along predefined pattern in the X-Y direction (Figure 1)[2]. Various configurations exist whereby the nozzle or collection plate are charged, all aiming to establish a net force between the nozzle surface tension and the attraction of an electrostatically charged droplet to the collector, which stabilises the fluid column and prevents the jet from undergoing Raleigh Plateau instabilities [3]. This enables control of defined laydown patterns and the diameter of the fibre [4]. The electric field imparted, and its subsequent electrical force, is impacted by the collector shape, morphology [5], material properties [6], and by the instrument configuration and process parameters [7, 8]. The direct writing of linear fibres is established when the computer-controlled collector speed is above than the ultimate jet speed, termed the critical translation speed (CTS). When operating well above this CTS the fibre can be stretched to obtain diameters down to submicrometer size, however when processing below this CTS value; nonlinear fluid patterns due to jet buckling are observed [9] .

Since 2015 there has been a substantial increase in publications documenting MEW due to the attractiveness of solvent-free approaches in creating micro-fibrous scaffolds. The ability to melt electrowrite candidate polymers is dictated by characteristics such as its molecular weight, melt flow index and thermomechanical properties [10]. Without question, the gold standard polymer for MEW is PCL due to its ease of fabrication, availability (including medical grade standard) and low range of melting temperatures [11]. This relatively soft polymer also renders a flexible scaffold with mechanical properties close to soft biological tissues and non-hazardous in vivo degradation rate [12].

MEW process parameters have been extensively investigated with CTS [13], collector speed, collector distance and pressure [14], polymer melt viscosity [10] and nozzle-exit-channel shape [11] all individually having a significant influence on printing and the resultant fibres being collected.

Melt electro written scaffolds are typically fabricated on flat or more recently; cylindrical mandrel collectors [15]. This fabrication on flat surfaces is primarily dictated by the electro-hydrodynamic working principle of MEW which relies on the use of a constant electric field to deposit fibres in well-organized 3D patterns [4]. Due to the semiconductive nature of many molten polymers, an excess charge from the nozzle is trapped within each deposited polymer fibre and subsequently counteracts accurate arrangement of successive fibres with increasing electrical repulsion per layer. Therefore, when printing above the initial induced charge threshold it is vital to at least maintain constant level of electrostatic forces [9]. MEW structures are largely deposited onto flat substrates as to prevent instabilities in the electric field strength. Establishing a balance between the various parameters has enabled advancement, such as production of large voluminous and highly ordered structures [16]. Such thicker scaffolds can be fabricated by adjusting height to achieve a consistent distance between the print head and the top of the sample while simultaneously incrementing the applied voltage [16]. Additionally, multiphasic MEW structures can be fabricated in a single step by adjusting the fibre diameter during printing [4].

Considering the current status-quo of MEW PCL scaffolds; retrospective conformation of a flat MEW patch to a 3D configuration, requires deformation, straining and/or plastic deformation of the PCL material which can impact the precision of scaffold porosity and mechanical performance thereafter. Living tissue structures are generally non-flat, therefore the possibility to MEW on non-flat surfaces could enable more applications and versatility to this technique. The reports of such application are sparse but are gradually gaining momentum [17, 18].

In this study, we seek to gain a more informed understanding of the electrostatic field underpinning MEW and the interplay between substrate material, topography and nozzle positioning when looking to print onto curved structures. This information will inform a more accurate fabrication of fibrous biomaterial scaffolds from flat to more anatomically conforming substrates. Through computational modelling, the effect of substrate electrical properties and geometry on the underlying electric field distribution and electrical force is investigated.

2. Results and Discussion

Nozzle height has a causal effect on the electric field strength.

Prior to investigating the effect of substrate geometry on print quality, we sought to understand the impact of MEW nozzle height on the electric field strength between the collector and the nozzle using computational modelling (Figure 2). A fine balance must be reached to achieve the optimal electric field density to maintain a stable polymer jet and reproducible printing during MEW [16]. Changes in the working distance imparted by 3D geometries can induce electric field variabilities and destabilisation of the fluid column which introduces printing defects. Insufficient electrostatic forces at the nozzle tip can lead to the unwanted accumulation of molten polymer material in the Taylor cone which is then dispersed as beading in the polymer jet [16]. The generation of electric sparking at the nozzle during printing can also occur in MEW and is reported in solution electrospinning [19, 20]. This sparking occurs when the electric field strength exceeds the dielectric breakdown strength of the surrounding medium, in the case of MEW, air. The breakdown strength of air is approximately 3×10^6 Vm^{-1}, which can fluctuate in response to humidity, pressure and the electrode geometry [21]. Corona discharge has also been reported in multiple EHD processes whereby the air surrounding a high voltage conductor, such as the charged collector in MEW, undergoes dielectric breakdown and becomes conductive. [22]. There is also a minimum value for the applied voltage (threshold voltage) necessary to pull a polymer jet from the Taylor cone at the nozzle [23].

Working distance has a noticeable impact on the overall electric field strength, with a concentration at the nozzle tip. For a non-uniform electric field, the relationship between voltage and electric field strength can be represented by the following formula:

Equation 1

$$E \propto -\frac{\Delta V}{\Delta s} \quad [22]$$

Where E = electric field strength (V/m), V = voltage (V) and Δs = distance over which the change in potential (ΔV) takes place (here the distance between the nozzle and collector). As distance s increases, the electric field strength (E) decreases accordingly. On average, a voltage of 7 – 7.5 kV is reported for MEW-printing of PCL [24]. At a continuous applied voltage of 7.5 kV, the relationship in Equation 1 is clearly illustrated in our COMSOL modelling where a nozzle collector distance of 5 mm results in an electric field strength of 3.67 x 10^6 Vm^{-1} at the edges of the nozzle tip which decreases to 2.01 x 10^6 Vm^{-1} for a nozzle distance of 15 mm. A higher voltage yields an expansion of the area experiencing higher electric field strength surrounding the nozzle tip.

In tandem, increasing the nozzle height in 0.5 mm increments from 5 mm to 15 mm while the applied voltage is kept constant at 7.5 kV was investigated. When printing multi-layered scaffolds, the substrate height increases with the printing of consecutive layers. Considering a constant voltage and this widening distance, the electric field strength will decrease. This relationship between nozzle height and electric field strength is similar to that observed by Wang et al. for needleless electrospinning, who noted a decrease in electric field strength as the collecting distance was increased [25]. It can be seen in Figure 2 that for an applied voltage of 7.5 kV, there is an exponential relationship between the electric field strength at the centre of the nozzle and nozzle height which we have modelled using equation 2:

Equation 2 $$E = 3937163\ EXP^{-0.2007H} + 1466131$$

Where E = electric field strength (Vm^{-1}) and H = nozzle height (mm).

The nozzle height also plays an important role in the formation of the Taylor cone and jet initiation. This can be understood from the basic principle of Coulomb's law [13]:

Equation 3 $$F = k_e \frac{q_1 q_2}{r^2}$$ [22]

Where k_e = Coulomb's constant (~8.988 x 10^9 Nm^2C^{-2}) , $q_1$and q_2 are the magnitudes of two point charges and r is the distance between them. As these electrostatic forces decrease, they may become insufficient to overcome the surface tension present in the polymer at the nozzle tip.

Applying a voltage of 7.5 kV and a nozzle height of 4 mm or less, it is likely that electrical sparking would occur at the nozzle tip due to electric field strengths exceeding the dielectric breakdown strength of air. For this particular model, with an applied voltage of 7.5 kV, it is recommended that the nozzle height is kept above 4 mm to avoid sparking in the system.

Based on our simulations up to now, printing on non-linear substrates would impact the electric field strength further with the risk of imprecise fibre deposition. Quite often in MEW, accurate fabrication of ordered fibrous and contoured microstructures is yielded from planar metallic substrates such as copper, stainless steel or aluminium [9, 17]. While reliable, a quick, low energy and scalable production of metallic substrates to serve as anatomical surfaces and moulds is lacking and lacks practicality when aiming to create ‚once-off' patient specific designs.

Curved contoured substrates impact electric field density and MEW accuracy.

Polylactic acid (PLA) is a relatively cheap and accessible material that can be easily used to produce complex anatomical relevant shapes in a time efficient manner and easily applied in the most conventional of 3D printer setups. To exploit MEW as a technique to produce fibrous scaffolds applicable to anatomically shaped configurations, it is fundamental to understand the effects of the electrical properties of the collecting material and its respective geometry on accurate fibre deposition. A proof-of-concept 3D substrate 'cap' was fabricated based on a 70 mm diameter model sphere design using a 5 mm cap of the sphere (resulting in a dome structure (Figure 3 (a-c))), used as a substrate mould for which the PCL fibres could be deposited onto. Although this geometry is relatively simple compared to complex organ or bone geometries, its curvature is higher than many organs found in the human body. One example application could be the surface of the heart where a set of procedures for evaluating regional left ventricle surface shape from anatomically accurate models reconstructed from cardiac magnetic resonance images is possible [26]. However, it is likely that there is a limiting curvature for which accurate fibre placement is possible.

During an initial MEW attempt on this substrate, as the nozzle traversed away from the dome centre towards the dome periphery (Figure 3d), an increased inaccuracy in fibre deposition occurred due to PCL fibre bending (Figure 3 (e-h) and Figure 4(f,g)). PCL fibre bending was initially attributed to an altered electric field strength on the PCL fibre due to the PLA substrate and caused the PCL fibre to take the least resistive route to ground and become more attracted to the PLA.

To understand this further we again employed COMSOL Multiphysics software to perform electric field simulations of the MEW setup with the domed collection mould present. The electric field strength at different positions upon this PLA mould was quantified to understand any variations in electric field strength that may impart this fibre bending at a continuous height which was unchanged (Figure 4 a-d). The point closest to the nozzle (position 3, where the centre of the mould was directly under the nozzle) exhibited the strongest electric field (1.08 x 10^6 Vm^{-1}). Position 1 (where the nozzle was directly above the edge of the mould) exhibited the weakest electric field strength (4.91 x 10^5 Vm^{-1}). The electric field plays a major role in MEW and governs important properties such as the flight path of the polymeric jet and fibre diameter [27]. The simulation conclusively demonstrates that the distance between the nozzle and the collector has a major effect on the electric field strength. This is in strong agreement with previous reports whereby the printing distance has been continuously adjusted to keep a constant distance [28-30]. Previously, Peiffer et al. maintained a constant distance to the collecting surface to achieve successful deposition of micro sized fibres on a 3D anatomically shaped collector surface with a unidirectional curved aspect [18]. Saidy et al. reported a stable jet formation by using a hybrid collector instead of a conventionally employed metallic one [17]. However, while a 3D geometric scaffold with a stable polymer jet was achieved, accurate placement of the PCL fibres in a 3D geometry was not nor was printing height adjusted.

Printing on curved contours requires adaptation of nozzle height.

Based on these observations, we initially considered that the PCL fibre was taking the shortest distance path from the nozzle to the PLA mould as the most direct trajectory to dissipate charge built up in the filament. If indeed the PCL fibre preferentially deposited via the shortest distance path, the nozzle position could potentially be accounted for and adjusted accordingly. Therefore, we sought to apply a shortest-distance trajectory designed for accurate fibre placement (Figure 5a). A MATLAB code was generated to map the nozzle position relative to the shortest distance the fibre would be drawn towards on the PLA mould (see S2-supplementary). This code facilitated a fixed distance (6 mm) which then outputted a table of values corresponding to all of the individual nozzle positions. Using this shortest-distance approach; while there was a slight improvement on print quality and accuracy in comparison to using an unchanging z-path (Figure 2); fibre bridging, and bending was still observed at the end of the dome. Nozzle position analysis was also performed to determine the change in horizontal direction that would occur when printing from the shortest distance. This analysis determined that for 3D mould used in this study, the further the distance from the centre of the dome, the larger the change in the absolute horizontal direction would be between the point directly below the nozzle and the point of closest absolute contact (supplemental). This could explain why fibres experience a much greater bending phenomenon at the edge of the mould to accurately deposit fibres in the desired position due to this large differential between.

It is reported in one previous MEW study that rapid changes in the working distance imparted by 3D metallic collectors causes electric field variabilities and consequent breakage of the fluid column leading to printing defects [17]. In such studies the voltage was specifically applied to the nozzle and the collector plate was grounded; whereas in our study the opposite is true as the nozzle is grounded and a high voltage is applied to the collector plate, although the previous study also used a combination of materials to create a hybrid collector [17]. Ideally an anatomical shaped collector should be composed of one material preventing the effect of different conductivity properties in multiple materials.

We also programmed the trajectory of the nozzle to continuously maintain a height of 6 mm directly above the surface of the curved substrate. Again, this was facilitated by a custom mathlab code to map the nozzle trajectory. In this instance, more accurate placement of fibres was noted at both the centre and in particular at the periphery of the dome.

Substrate/mould material impacts on fibre deposition.

Scaffolds MEW printed on conductive and non-conductive substrates have been shown to possess a negative and positive residual charge, respectively [19]. More residual (positive) charges remain in PCL fibres deposited on the non-conductive substrate than those on the conductive substrate, as evidenced by the repulsion phenomenon between fibres on a non-conductive substrate and attraction on a conductive substrate. Therefore, the PCL fibre bending configuration in our study appears consistent with the literature but may not be only due to the altered electric field imparted by the substrates. PCL fibres becoming built up with residual charge and experiencing a repulsion phenomenon as the charge was not being transferred to the PLA material. This could be why we do not see sequential stacking of MEW fibres when applying the shortest distance method.

To investigate this further we considered the percentage infill of the 3D printed PLA mould with infills of 10% and 90%. A 10% PLA infill resulted in neat stacking of deposited PCL fibres with minor inaccuracies in the final print (Figure 5). A 90% PLA infill resulted in PCL discordant stacking of fibres onto one another (Figure 5). This result is consistent with previous reports that detail PCL fibres experiencing a repulsion phenomenon when deposited on a non-conductive substrate and attraction on a conductive substrate [19, 31]. The positively charged PCL fibre transfers charge carriers to the substrates. A conductive substrate has greater capacity to allow charge transport to the ground/substrate surface when compared to a non-conductive substrate. This result leads to the assumption that the extra PLA filament within the 90% infill PLA produces more of an insulator effect than the 10% infill, resulting in a greater build-up of charge in the PCL fibres, thus creating a greater charge force to separate the PCL fibres and prevent the accurate stacking of layers.

There are many important observations in this study that warrant commenting upon. One must acknowledge that the while somewhat simplistic and perfectly ordered the COMSOL modelling clearly remonstrates the impact of applied voltage and nozzle/collector distance on fibre control and deposition. Yet, there are several other considerations to be taken with this. The ability of the collector to minimise residual charges will impact fibre deposition and careful consideration could obviate complex obviation of z-axis trajectory, which is especially important for more advanced contours.

Overall, analysis of pore size finds lower deviation at the centre when compared to the periphery of the dome. This suggests that there may be a limit on the curvedness of which can be printed onto. Regardless, there are still numerous biomedical applications with a favourable geometry that would benefit from a three-dimensional melt electro written patch.

3. Conclusion

The objective of this study was to fabricate melt electro written scaffolds onto curved non-linear substrates while maintaining controlled placement of the polymer fibre. The in silico electric field model was simulated in COMSOL Multiphysics software. The electric field strength increased significantly when the nozzle moved over the PLA mould while the electric field strength remained relatively constant moving over the aluminium mould. The electric field strength at different positions on the PLA mould was also investigated. The point on the PLA mould closest to the nozzle exhibited the strongest electric field confirming that the distance between the nozzle and collector has a major effect on the electric field strength.

Accurate fibre deposition on a curved PLA dome was successful, yet only when maintaining a constant electrostatic force constant through a uniform vertical height to the collecting surface. MEW fibre deposition is strongly affected by the materials they are printed on. The electrical properties of the collector materials revealed that the less conductive it is, the greater the amount of charge remains in the polymer fibres resulting in a repulsion phenomenon. Repulsion of the PCL fibres was observed by the uneven stacking of PCL fibre layers. Greater fibre separation resulted in the 90% PLA infill rather than the 10% PLA infill.

Overall, this study establishes the groundwork for the further translation of the merging of MEW and bioprinting, from flat to anatomical relevant 3D structures, that the regenerative medicine and biofabrication fields aim to recreate.

4. Experimental Section/Methods

Electric Field Simulation: The in silico electric field model was simulated in COMSOL Multiphysics software (version 5.4, COMSOL Inc., United States). The MEW setup was modelled as a 2D configuration and the electrical conductivity of the materials defined according to the physical properties of materials established in the COMSOL Metaphysics (Stainless steel collector plate and nozzle: 4.032e6 Sm^{-1}, Air: 5e-15 Sm^{-1}, Aluminium 3.774e7 Sm^{-1}) while the dielectric constant of 3D printed PLA was taken from previously published papers (die-electric constant: 3.471) [32]. The electric field strength during the MEW process was modelled by defining the nozzle position at a collector distance of 10 mm from the collector plate. The collector plate was assigned a voltage of 7.5 kV while the nozzle was grounded. A detailed guide on the COMSOL setup is provided in Supplemental Part 1 (S1).

MEW Fabrication of Scaffolds: Fibres of poly(ε-caprolactone) (Mw 74 kDa, PCL, LACTEL Absorbable Polymers) were fabricated via MEW using a commercially available instrument (MELT A-1204- 0001-01D, Spraybase, Dublin, Ireland, Figure 1). MEW was performed at ambient conditions (not controlled), temperature 23–27 °C (accuracy ± 0.5 °C) and relative humidity 31–37% (accuracy ± 3% RH). Printed scaffolds were lifted from the collector by using forceps.

PCL was loaded into the stainless-steel reservoir fitted with a 0.5 mm diameter stainless steel nozzle. All patches were fabricated at a constant melting temperature of T = 85 °C. The device remained at this temperature for at least 30 minutes before printing to remove any air bubbles from the polymer melt. The voltage and pressure were set as 7.5 kV ± 0.001 and 0.150 ± 0.03 bar respectively for all PCL scaffolds.

Scaffold designs were drawn using the SEL Program Generator (IAI America, Inc.) software. This software allows the user to generate the nozzles path by defining the X,Y and Z position of the nozzle at any given point. The software then automatically generates a SEL program and a table of positions file which are then imported into the XSEL PC software (IAI America, Inc.). The SEL program and position file are then uploaded to the axis-positioning controller of the stage collector (X,Y direction) and the nozzle motor (Z direction).

Melt electrospun PCL square-mesh scaffolds were fabricated based on a design of 48 mm x 48 mm grid with fibre spacing of 2 mm (Figure 3). The loops at the edge of the mesh were to prevent the print from becoming jagged as this would result in the fibres not stacking perfectly and could potentially cause structural weaknesses. The number of layers was set to 10. The scaffolds were fabricated with constant collector speed of 40 mms^{-1}. The nozzle height was kept constant at 8 mm throughout the print.

3D square-mesh design (non-adjusting z-axis): Scaffolds using the MEW parameters described above. The nozzle path (Figure 3) was kept at a constant distance of 8 mm above the steel plate throughout the print. The PLA dome structures were sprayed with Ethanol 70% before the printing process to prevent the sticking of the PCL to the PLA structures.

3D square-mesh using shortest distance method: The scaffolds printed for the shortest distance method were fabricated with the same MEW parameters as the control mesh. The nozzle path (Figure 5) would be kept at a constant distance of 6 mm from the PLA structure throughout the print. Scaffolds were sprayed with Ethanol 70% following the completion of the print to ease removal.

The calculation to find the position of the nozzle for this method differs from the vertical distance method. To calculate the position of the nozzle at a defined shortest distance from the PLA dome, a perpendicular line must be drawn from the dome's surface to a point in space. For the geometry used in this study, the perpendicular (shortest distance) line results in being an extension of the original radius of the PLA dome (Figure 5). Therefore, by extending the original radius by a defined 6 mm, the nozzle path can be identified for the shortest distance. A

MATLAB code was created to calculate the coordinates of the nozzle position. The MATLAB code produced a list of nozzle coordinates which were then manually inputted into the SEL Generator software to define the nozzle position throughout the print.

3D square-mesh using adapting distance: The scaffolds printed for the vertical distance method were fabricated with the same MEW parameters as the control mesh. The number of layers was set to 10. The nozzle path (Figure 5) would be kept at a constant vertical distance of 6 mm above the PLA dome structure throughout the print. The PLA dome structures were sprayed with Ethanol 70% before the printing process to prevent the sticking of the PCL to the PLA structures.

The position of the nozzle at a given point was calculated using the equation of a sphere:

$$x^2 + y^2 + z^2 = r^2$$

As the dome structure was constructed from a sphere of radius 35 mm, this value can be substituted in for r. By adding 30 to the z part of the equation, the sphere can be seen to have a height of 5 above the y-axis, which represents the height of the PLA dome above the stainless-steel plate of the MEW. If the X and Y coordinate are predetermined at a given point in space, then the final variable of the equation (z parameter) can be found. By subbing in the X and Y values, the height of the dome at any given point can be calculated.

Once the Z positions of the PLA dome were calculated, a vertical distance (z axis) of 6 mm was added to define the position of the nozzle. This allowed the position of the nozzle to constantly be a vertical distance of 6 mm away from the PLA dome. The scaffolds were fabricated with constant collector speed of 40 mms^{-1}.

Supporting Information

Supporting Information is available from the Wiley Online Library or from the author.

Acknowledgements

This work was supported by the Department of Mechanical, Manufacturing and Biomedical Engineering at Trinity College Dublin. The authors would like to thank Profs John Kennedy and Seamus O'Shaughnessy, Dr Michael Gibbons and the general Monaghan Lab at Trinity Centre for Biomedical Engineering for their input and advice.

Received: ((will be filled in by the editorial staff))
Revised: ((will be filled in by the editorial staff))
Published online: ((will be filled in by the editorial staff))

References

[1] Castilho, M., et al., *Melt electrospinning writing of poly‐Hydroxymethylglycolide‐co‐ε‐Caprolactone‐based scaffolds for cardiac tissue engineering.* Adv Healthc Mater, 2017. **6**(18): p. 1700311.

[2] Afghah, F., et al., *Biomimicry in bio-manufacturing: developments in melt electrospinning writing technology towards hybrid biomanufacturing.* App Sci, 2019. **9**(17): p. 3540.

[3] Stachewicz, U., et al., *Surface free energy analysis of electrospun fibers based on Rayleigh-Plateau/Weber instabilities.* Eur Pol J, 2017. **91**: p. 368-375.

[4] Hrynevich, A., et al., *Dimension‐based design of melt electrowritten scaffolds.* Small, 2018. **14**(22): p. 1800232.

[5] Wang, B., et al., *Impact of substrate geometry on electrospun fiber deposition and alignment.* Journal of Applied Polymer Science, 2017. **134**(19).

[6] Yan, H., L. Liu, and Z. Zhang, *Alignment of electrospun nanofibers using dielectric materials.* Applied Physics Letters, 2009. **95**(14): p. 143114.

[7] Wunner, F.M., et al., *Printomics: the high-throughput analysis of printing parameters applied to melt electrowriting.* Biofabrication, 2019. **11**(2): p. 025004.

[8] Brown, T.D., et al., *Melt electrospinning of poly (ε-caprolactone) scaffolds: Phenomenological observations associated with collection and direct writing.* Materials Science and Engineering: C, 2014. **45**: p. 698-708.

[9] Robinson, T.M., D.W. Hutmacher, and P.D. Dalton, *The Next Frontier in Melt Electrospinning: Taming the Jet.* Advanced Functional Materials, 2019. **29**(44).

[10] Ko, J., et al., *Effects of molecular weight and temperature on fiber diameter of poly (ε-caprolactone) melt electrospun fiber.* Journal of the Korean Society of Manufacturing Technology Engineers, 2015. **24**(2): p. 160-165.

[11] Esmaeilirad, A., et al., *The effect of nozzle-exit-channel shape on resultant fiber diameter in melt-electrospinning.* Materials Research Express, 2017. **4**(1): p. 015302.

[12] Bartnikowski, M., et al., *Degradation mechanisms of polycaprolactone in the context of chemistry, geometry and environment.* Progress in Polymer Science, 2019. **96**: p. 1-20.

[13] Tourlomousis, F., et al., *Melt electrospinning writing process guided by a "Printability Number".* Journal of Manufacturing Science and Engineering, 2017. **139**(8).

[14] Dayan, C.B., et al., *Modeling 3D melt electrospinning writing by response surface methodology.* Materials & Design, 2018. **148**: p. 87-95.

[15] Tadayyon, G., D.J. Kelly, and M.G. Monaghan, *Extrusion-Based Additive Manufacturing Techniques for Biomedical Applications*, in *Reference Module in Materials Science and Materials Engineering*. 2021, Elsevier.
[16] Wunner, F.M., et al., *Melt Electrospinning Writing of Highly Ordered Large Volume Scaffold Architectures.* Adv Mater, 2018. **30**(20): p. e1706570.
[17] Saidy, N.T., et al., *Melt Electrowriting of Complex 3D Anatomically Relevant Scaffolds. Front. Bioeng. Biotechnol.*, 2020. **8**: p. 793.
[18] Peiffer, Q.C., et al., *Melt electrowriting onto anatomically relevant biodegradable substrates: Resurfacing a diarthrodial joint.* Mater Des, 2020. **195**: p. 109025.
[19] Ding, H., et al., *A fundamental study of charge effects on melt electrowritten polymer fibers.* Materials & Design, 2019. **178**: p. 107857.
[20] Reneker, D.H. and A.L. Yarin, *Electrospinning jets and polymer nanofibers.* Polymer, 2008. **49**(10): p. 2387-2425.
[21] Rigden, J.S. and B. Pippard, *Macmillan encyclopedia of physics.* Physics Today, 1997. **50**(9): p. 65.
[22] Urone, P. and R. Hinrichs, *College physics.* 1998.
[23] Dalton, P.D., *Melt electrowriting with additive manufacturing principles.* Current Opinion in Biomedical Engineering, 2017. **2**: p. 49-57.
[24] Kade, J.C. and P.D. Dalton, *Polymers for Melt Electrowriting.* Advanced Healthcare Materials, 2021. **10**(1): p. 2001232.

Figure Legends:

Figure 1. Overall study design to MEW fibrous scaffolds on curved contours whereby electric field strength simulation highlights the distortion of electric field strength within setup and discordant fibre deposition requiring the continuing adjustment of nozzle height to achieve accurate fibre deposition.

Figure 2. Electric Field Strength (Vm^{-1}) simulation for varying nozzle height (mm) in MEW. (a) 2D surface plot of simulation results depicting the electric field strength ($^{-1}$) for constant voltage of 7.5 kV and nozzle height of 5 mm, (b) 8 mm, (c) 12 mm and (d) 15 mm. (e) Profile of Electric Field Strength at nozzle calculated at various horizontal (x) positions along length of collector while nozzle is positioned at origin x = 0, height is increased from 5 mm to 15 mm (in 0.5 mm increments) with voltage is constant at 7.5 kV. (f) Profile of Electric Field Strength at collector plate at various x positions along length of collector while nozzle is positioned at x

= 0, height is increased from 5 mm to 15 mm (in 0.5 mm increments) with voltage is constant at 7.5 kV. (g) Trends of Electric Field Strength (V/m) calculated along the distance between nozzle and collector various values of separation between nozzle and collector and constant voltage of 7.5 kV.

Figure 3. Initial approach of MEW printing on defined curvature. (a-c)) depicts the overall design, shape and printed cap of height 5 mm obtained from a sphere of radius 35 mm. (d) trajectory of nozzle as it traverses across the curved PLA structure with working distance ranging from 8 mm above the steel collector to 3 mm at the centre peak of the curved PLA. (e) resultant MEW patch showing the curved contour imparted by the PLA contour with magnified micrographs (f) showing the edge of the patch and (g) centre of the patch with noticeable fibre bending and discordant fibre stacking. (h) quantification of pore size at the edge and centre from micrographs, data displayed is the mean ± standard deviation. No significant difference was detected between the pore size at the centre versus the edge of the patch (students t-test, $n=3$, $p<0.05$)

Figure 4. Impact of substrate height and nozzle height on fibre deposition. (a) fibre deposition when directly above stainless steel collecting plate versus (b) fibre deposition and bending when traversing across PLA substrate. (c) plot of Electric field strength versus spatial distribution of electric field strength according to nozzle position away from centre zero illustrated in (d) as nozzle moves from edge position 1 in (e), middle position 2 in (f) and centre position 3 in (g).

Figure 5. Approaches for more accurate fibre deposition on curved surface PLA mould. (a) schematic of vertical height adjustment in order to facilitate accurate fibre deposition via the shortest distance between the nozzle tip and curved surface with (b) illustrating a map of coordinates generated via MATHLAB code in supplemental information. (c, d) micrographs of generated patches with close up of (c) centre and (f) edge regions indicating attraction between fibre layers and inaccurate deposition. (g) quantification of pore size at the edge and centre

from micrographs, data displayed is the mean ± standard deviation. No significant difference was detected between the pore size at the centre versus the edge of the patch (students t-test, n=3, $p<0.05$). (h) schematic of vertical height adjustment in order to facilitate accurate fibre deposition by maintaining a distance of 6 mm vertically directly between the nozzle tip and curved surface with (i, j) micrographs of generated patches with close up of (k) centre and (l) edge regions indicating good stacking between fibre layers and accurate deposition. (m) quantification of pore size at the edge and centre from micrographs, data displayed is the mean ± standard deviation. No significant difference was detected between the pore size at the centre versus the edge of the patch (students t-test, n=3, $p<0.05$).

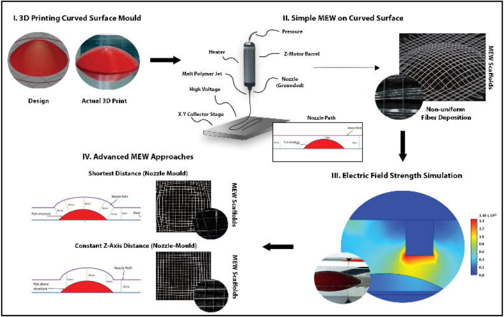
I. 3D Printing Curved Surface Mould
Design
Actual 3D Print
II. Simple MEW on Curved Surface
Pressure
Heater
Z-Motor Barrel
Melt Polymer Jet
Nozzle (Grounded)
High Voltage
X-Y Collector Stage
Nozzle Path
PLA structure
MEW Scaffolds
Non-uniform Fiber Deposition
III. Electric Field Strength Simulation
IV. Advanced MEW Approaches
Shortest Distance (Nozzle Mould)
Nozzle Path
PLA structure
Steel
MEW Scaffolds
Constant Z-Axis Distance (Nozzle-Mould)
Nozzle Path
PLA dome structure
MEW Scaffolds

Electric Field Strength (V/m) Simulation for Varying Nozzle Height (mm) in MEW

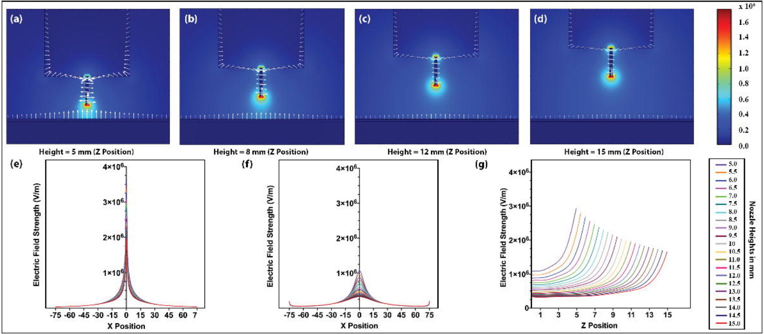

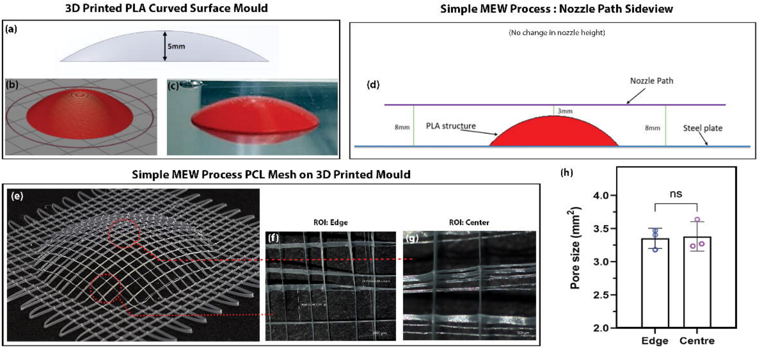
3D Printed PLA Curved Surface Mould
(a)
5mm
(b)
(c)
Simple MEW Process : Nozzle Path Sideview
(No change in nozzle height)
(d)
Nozzle Path
3mm
8mm
PLA structure
8mm
Steel plate
Simple MEW Process PCL Mesh on 3D Printed Mould
(e)
ROI: Edge
(f)
ROI: Center
(g)
(h)
ns
Pore size (mm²)
4.0
3.5
3.0
2.5
2.0
Edge
Centre

Electric Field Strength (V/m) Simulation for Varying Nozzle Position (mm) over 3D Printed Mould

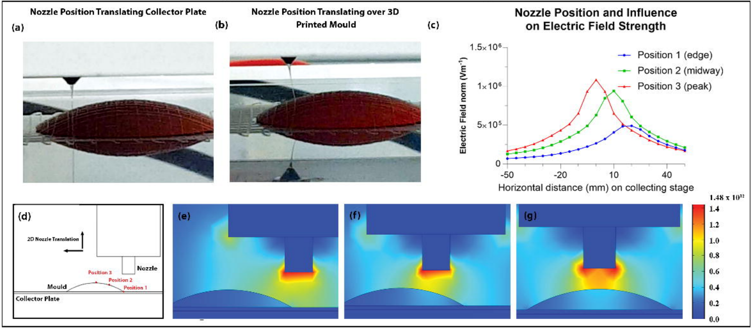

Advanced Melt-Electrowriting Approches for Curved Surface Mould